Supplementary Material: Electron-Nuclear Interaction Tensor (*T*) for a Proton Dipole-Coupled to an antiferromagnetically-coupled [*S* =5/2;*S* =2] Binuclear Center

Intermediate **X** is a diiron $S = ½$ center comprised of an Fe^{III}($S = 5/2$) ion antiferromagnetically coupled to a Fe^{IV}($S = 2$) ion.[27] As has been discussed extensively (see[12]), a nucleus of a diiron center that has through-space dipolar coupling to the individual ferric and ferryl iron ions of, $\boldsymbol{T}^{\mathbf{Fe(III)}}$ and $\boldsymbol{T}^{\mathbf{Fe(IV)}}$, respectively, will have an observed cluster dipolar coupling matrix to the cluster spin, $\boldsymbol{T}$, that is a weighted sum of the individual-ion interactions (**eq. S1**),

$$\boldsymbol{T} = \frac{7}{3}\boldsymbol{T}^{\mathrm{Fe(III)}} - \frac{4}{3}\boldsymbol{T}^{\mathrm{Fe(IV)}} \qquad \textbf{(S1)}$$

with a similar equation applicable when $\boldsymbol{T}$ is replaced by $\boldsymbol{A}$. To treat the dipolar interaction, we considered a nucleus at an arbitrary location, as depicted in **Fig 3**, took the classical form of the point-dipole interaction with the individual uncoupled iron ions, ($\boldsymbol{T}^{\mathbf{Fe(III)}}$ and $\boldsymbol{T}^{\mathbf{Fe(IV)}}$), expressed them in a common axis frame of **Fig 3**, and added them according to **eq. S1** to obtain the effective dipolar tensor $\boldsymbol{T}$ for the $S = ½$ ground state Hamiltonian of the spin-coupled cluster system. To carry **this out, it** is convenient to define a right-handed coordinate frame (***e***), the unit vectors of which are: e_3, lying parallel to Fe-Fe; e_1, lying in the Fe(H)Fe plane perpendicular to e_3; and e_2, normal to the plane, **Fig 3**. As expressed in this frame, the cluster dipolar interaction matrix takes the form given in **eq. S2**:

$$\mathbf{T} = \begin{pmatrix} T_1\cos^2\gamma + T_3\sin^2\gamma & 0 & (T_1 - T_3)\sin\gamma\cos\gamma \\ 0 & T_2 & 0 \\ (T_1 - T_3)\sin\gamma\cos\gamma & 0 & T_1\sin^2\gamma + T_3\cos^2\gamma \end{pmatrix} \qquad \textbf{(S2)}$$

This corresponds to the matrix for an interaction with principal values, $\boldsymbol{T} = [T_1, T_2, T_3]$, where the

hyperfine frame is rotated relative to the molecular [e_1, e_2, e_3] frame by a rotation around e_2 through the angle γ. This dipolar interaction matrix depends on the metrical parameters for the center and we chose to parameterize $\boldsymbol{T}$ for a given geometry of Fe(H)Fe in terms of r_1; r_1 is the distance between the Fe^{III} and the proton, $d_{Fe\text{-}Fe}$ is the Fe-Fe distance, and β_1 is the angle subtended by the Fe^{III}-H and Fe-Fe vectors (**Fig 3**). The principal values of the dipolar interaction tensor $\boldsymbol{T}$ then are given by **eq. S3**:

$$T_1 = \frac{1}{2}\left[\left(\frac{t_1 + t_2}{2}\right) + \frac{3}{2}\frac{1}{\cos 2\gamma}\left(t_1 \cos 2\beta_1 + t_2 \cos 2\beta_2\right)\right]$$
$$T_2 = -\frac{1}{2}\left(t_1 + t_2\right) \qquad \textbf{(S3)}$$
$$T_3 = -\left(T_1 + T_2\right)$$

where,

$$t_1 = \frac{7}{3}\left(\frac{2g\beta g_n \beta_n}{r_1^3}\right) \qquad t_2 = -\frac{4}{3}\left(\frac{2g\beta g_n \beta_n}{r_2^3}\right) \qquad \textbf{(S4)}$$

$$\tan 2\gamma = \frac{[t_1 \sin 2\beta_1 + t_2 \sin 2\beta_2]}{[t_1 \cos 2\beta_1 + t_2 \cos 2\beta_2]}$$

With these equations it is possible to calculate $\boldsymbol{T}$ for a proton at any position relative to the Fe-Fe framework; with the possible inclusion of an isotropic coupling term, this in turn allows us to simulate a 2-D set of ENDOR spectra for the proton at multiple fields across the EPR envelope. Calculations with these formulae show that when the proton lies outside of the region between the two iron ions ($\beta_1 > 90$ or $\beta_2 < 90$), namely when it is part of a terminal ligand to one ion, then to a good approximation this result

reduces to a point-dipole interaction with the adjacent iron. When the nucleus is located symmetrically relative to the two iron ions, namely when it is associated with an hydroxo (or aquo) bridge, then these results reduce to those reported previously.[23]

Use of HLLN(2) to compute ^{2}H ENDOR spectra of Hypothetical X with both T and B deuterons.

To sum the computed spectra for the **B**-proton of **HLLN(2)** with the experimentally generated simulation for the **T**-proton, requires that that the hyperfine tensor for **B**, $\boldsymbol{A_B}$, ($\boldsymbol{T_B}$) be expressed relative to the $\boldsymbol{g}$-tensor frame. This was done through a sequence of relationships. *(i)* Simulation of the experimental spectra (**Fig 4A**, **Table 1**) directly yields the **T**-proton experimental hyperfine and dipolar tensors, $\boldsymbol{A_T^{ex}}$, $\boldsymbol{T_T^{ex}}$, in the $\boldsymbol{g}$ frame. *(ii)* Taking the orientation of $\boldsymbol{T_T^{ex}}$ to correspond to that of the dipolar interaction for either one of the terminal deuterons if the H_2O ligand of **HLLN(2)**, as calculated with **eqs S1-4**, then gives the orientation of $\boldsymbol{A_T^{ex}}$, $\boldsymbol{T_T^{ex}}$ relative to the molecular $\boldsymbol{e}$ frame. *(iii)* Together, these relationships fix the orientation of $\boldsymbol{g}$ in the $\boldsymbol{e}$ frame (**Fig S7**), and thus the orientation of the dipolar interaction of the **HLLN(2)**, **B**-proton, $\boldsymbol{T_B}$, as calculated with **eqs S1-4**, relative to $\boldsymbol{g}$ (**Fig S7**).

A limitation to this procedure is that the experimental determination of the orientation of $\boldsymbol{A_T^{ex}}$ relative to the $\boldsymbol{g}$ frame contains degeneracy. In the present case this leads to two very distinct solutions[39] for the orientation of $\boldsymbol{g}$ in the $\boldsymbol{e}$ frame for each of the two choices of H_2O proton in **HLLN(2)**, and thus for the orientation of $\boldsymbol{A_B}$ relative to $\boldsymbol{g}$; these are listed in **Table S2.** All of the resulting four alternative assignments were tested by comparing experiment with their predicted 2-D ENDOR patterns for a hypothetical **X** that contains a **B-** as well as a **T**-deuteron, in analogy to the comparisons of **Fig 4C** and **Fig 5**. We find that the results for the two alternatives associated with H1 have a correspondence to those of H2, so show only those for H1. As seen in **Figs S4 and S5**, it is obvious that none of the additional intensity predicted for a **B-**deuteron by any of the model computations is present in experimental spectra.

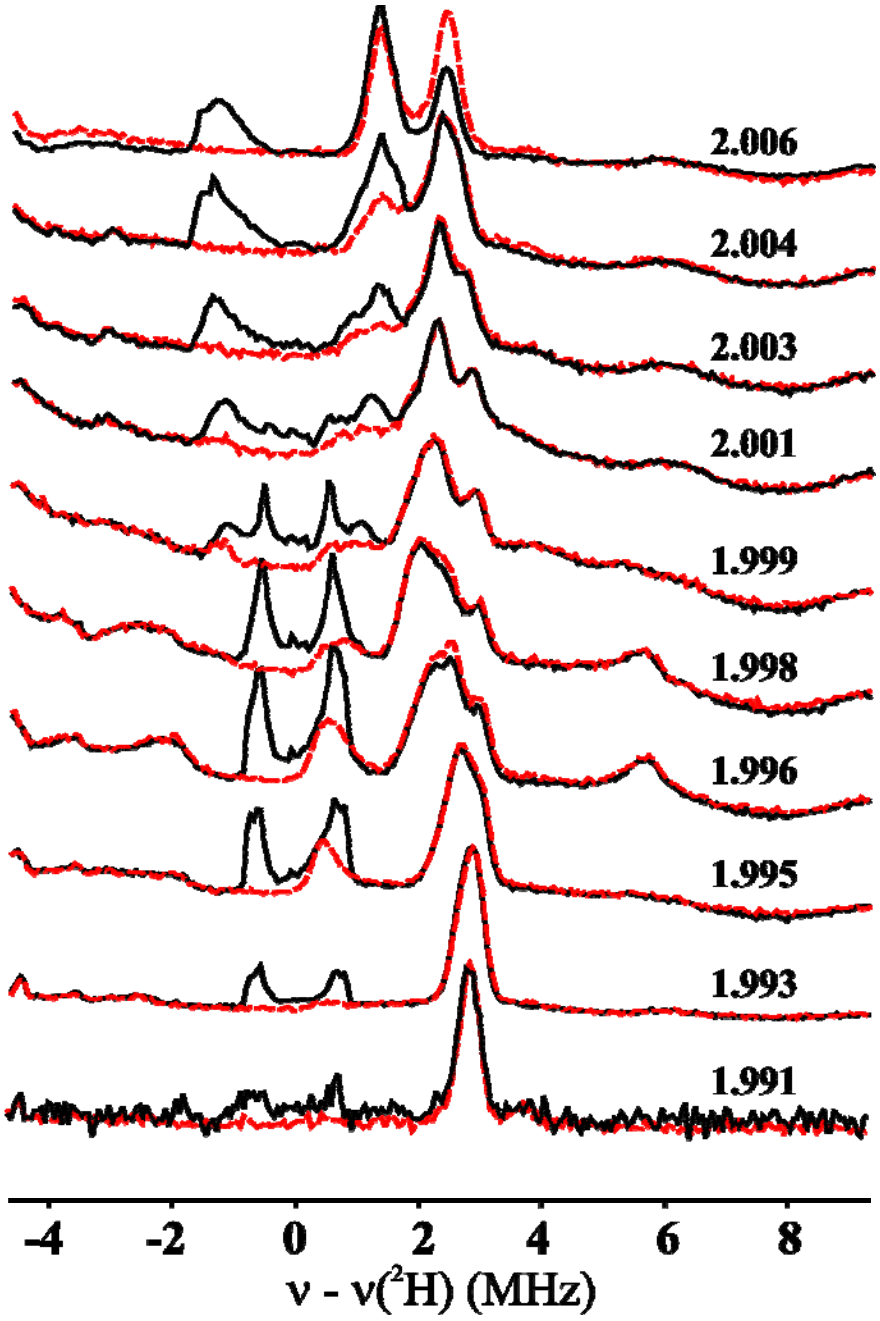

Fig S1:

Comparisons of the Davies ^{2}H ENDOR spectra of **X**(WT) in H_2O (red; 33 ms) and D_2O (black; 33ms). Experimental conditions: π pulse length = 200 ns, τ = 600 ns, repetition time = 50 ms, average MW frequency = 34.827 GHz, T = 2 K.

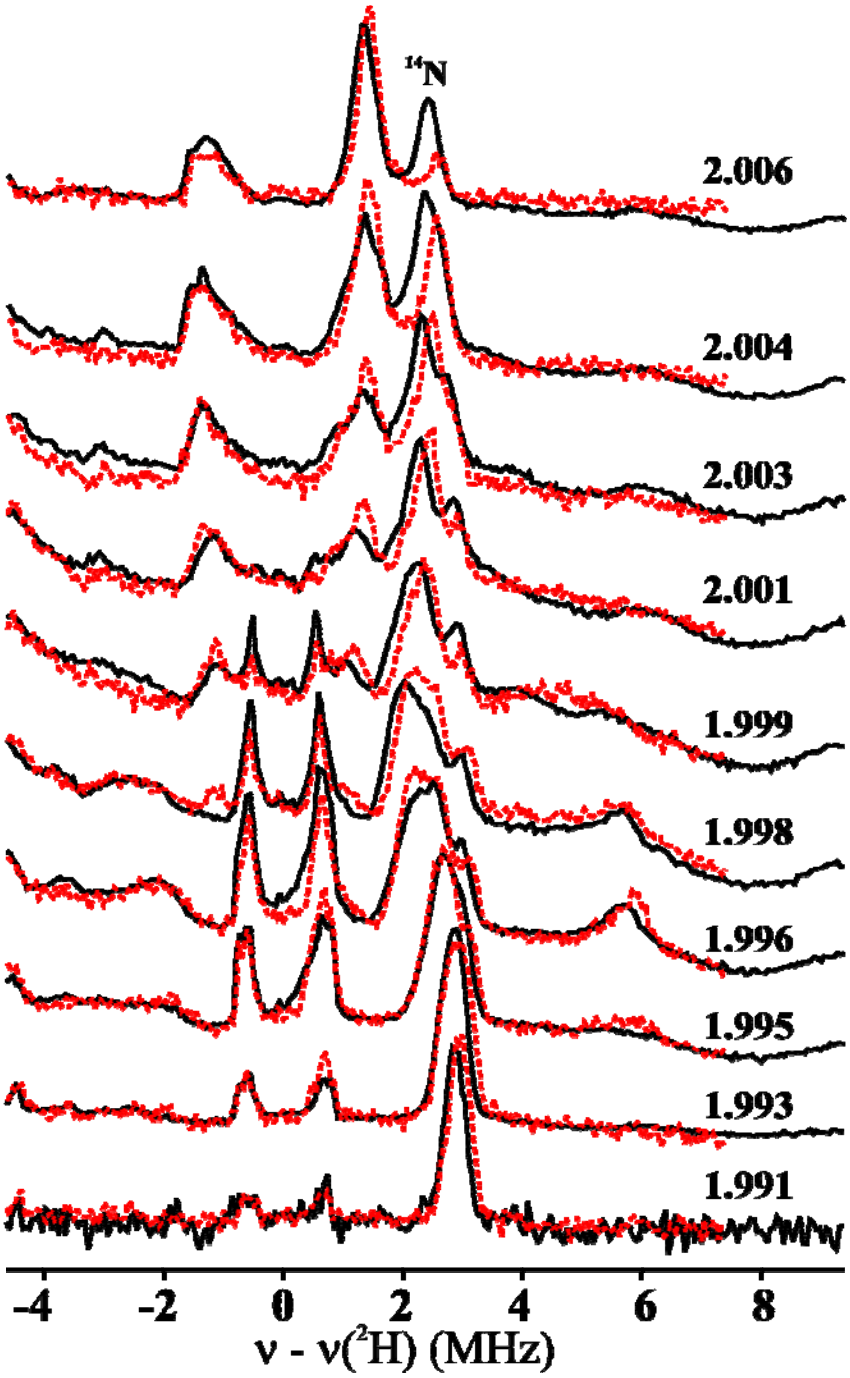

Fig S2A:

Comparisons of the Davies ^{2}H ENDOR spectra of **X**(WT; 33 ms; black) and **X**(Y-122F; 1.2 s; red) in D_2O; Experimental conditions: π pulse length = 200 ns, τ = 600 ns, repetition time = 50 ms, average MW frequency = 34.827 GHz, T = 2 K.

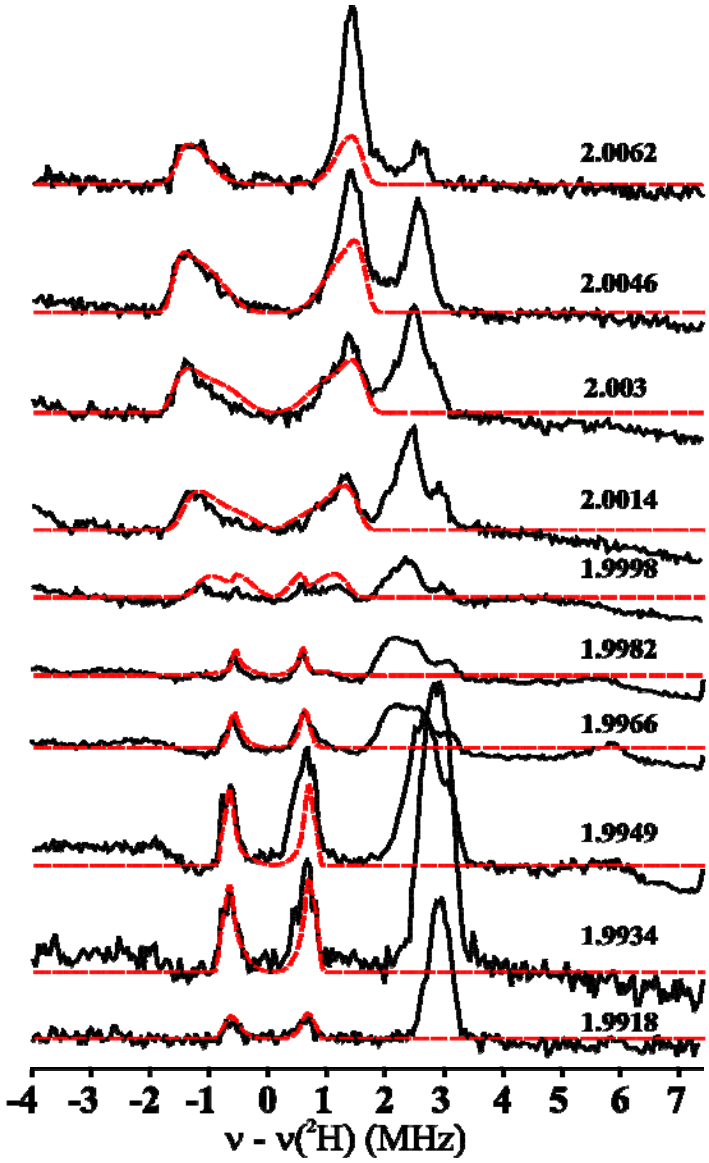

Fig S2B:

Simulated (red) and experimental (black) 2-D field-frequency plot of Davies ^{2}H ENDOR spectra of **X**(Y-122F; 1.2 s) in D_2O (^{2}H): Conditions: π pulse length = 200 ns, τ = 600 ns, repetition time = 50 ms, MW frequency = 34.774 GHz, T = 2 K. Simulation parameters (determined as described in text): $\boldsymbol{g}$ = [g_1 = 2.0056, g_2 = 1.9977, g_3 = 1.993], $\boldsymbol{A}$ = [A_1 = -1.55, A_2 = -1.15, A_3 = 3.2] MHz (Euler angles α = 10.5°, β = 74°, γ = 0), line widths used = 0.09 (minimum) to 0.25 (maximum) MHz. all spectra are centered at the ^{2}H nuclear Larmor frequency.

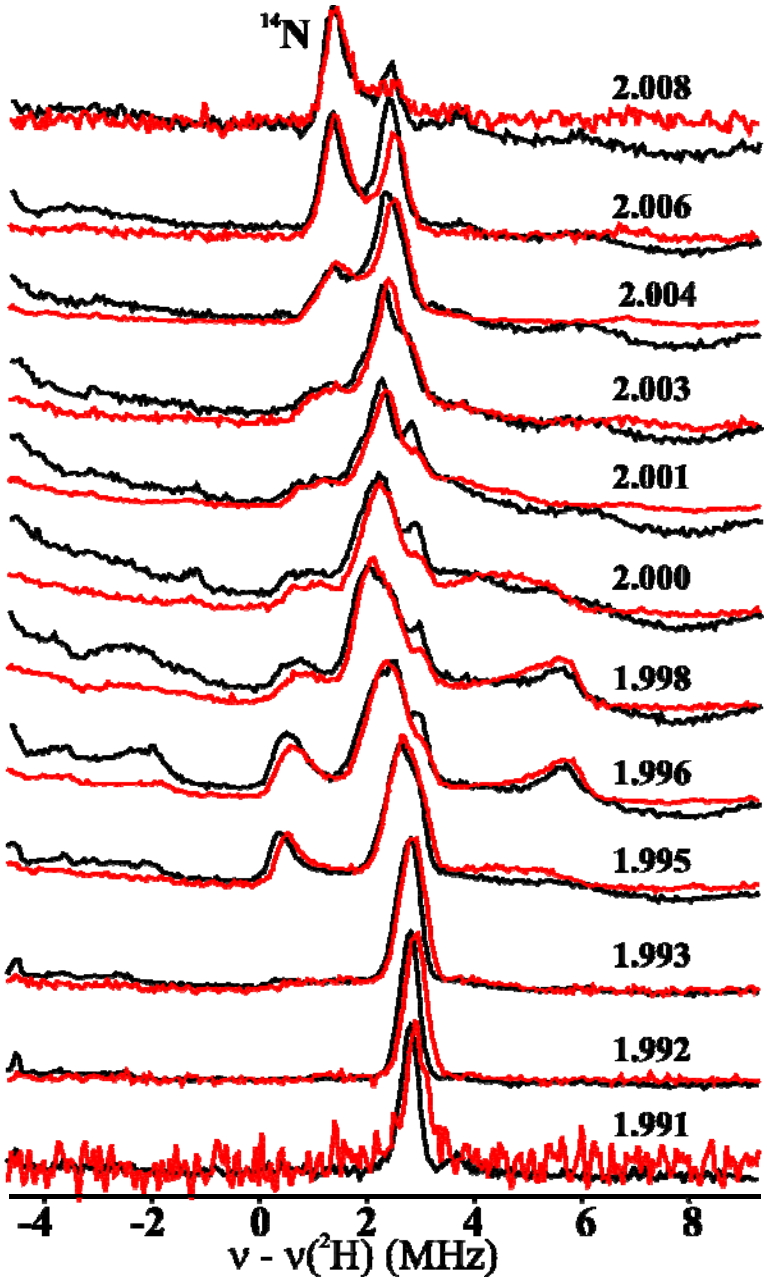

Fig S3:

Comparisons of the Davies ^{14}N ENDOR spectra of **X** (WT; 33 ms; black) and **X** (Y-122F; 610 ms; red) in H_2O; Experimental conditions: π pulse length = 200 ns, τ = 600 ns, repetition time = 50 ms, average MW frequency = 34.827 GHz, T = 2 K.

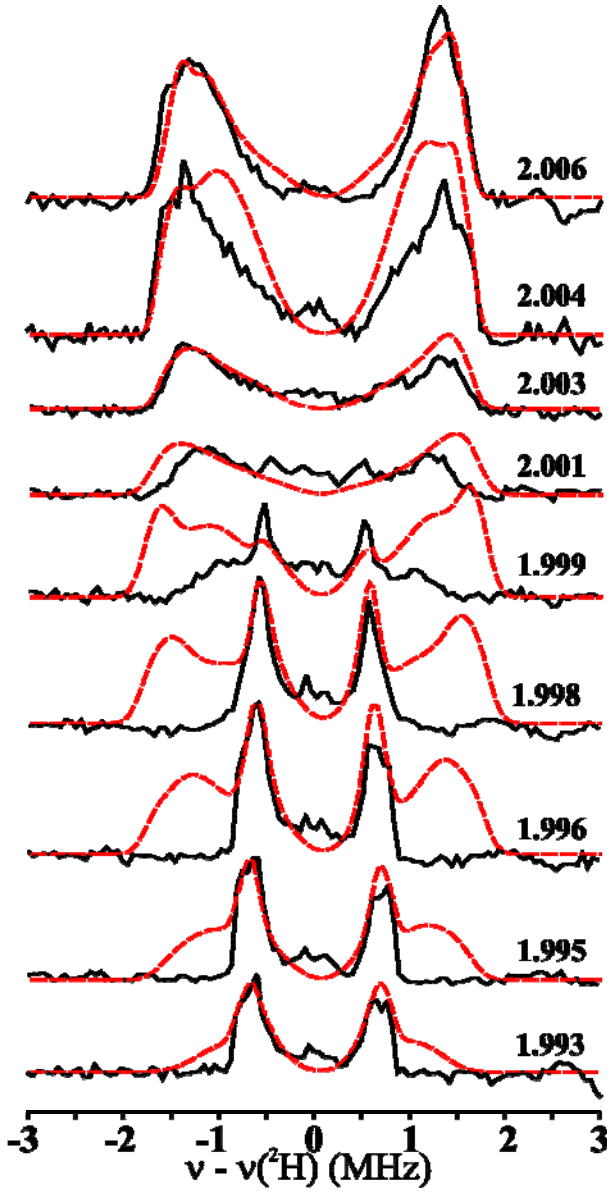

Fig S4:

Simulated [red; additions of the ENDOR spectra of the terminal and the bridging hydroxides; $\beta = +72^{\circ}$] and the experimental (black, background subtracted) 2-D field-frequency plot of Davies ^{2}H ENDOR spectra of RNR intermediate **X** (WT; 33 ms**)** in D_2O (^{2}H). Simulated parameters for the terminal (see **Fig 4A** and **Table 1**) and bridging hydroxides: $\boldsymbol{g}$ = [g_1 = 2.0056, g_2 = 1.9977, g_3 = 1.993], $\boldsymbol{T}$ = [T_1 = -3.387, T_2 = -0.24, T_3 = 3.627] MHz (Euler angles $\alpha = 48.4^{\circ}$, $\beta = 54.8^{\circ}$, $\gamma = 69.5^{\circ}$).

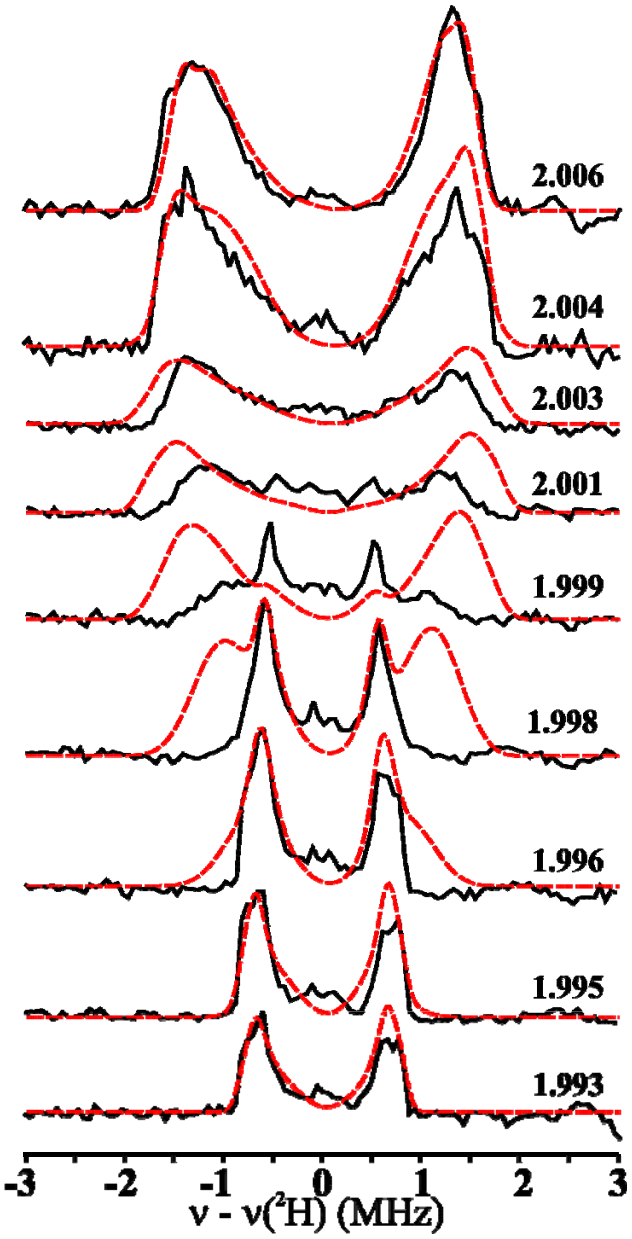

Fig S5:

Simulated [red; additions of the ENDOR spectra of the terminal and the bridging hydroxides; $\beta = -72^{\circ}$] and the experimental (black, background subtracted) 2-D field-frequency plot of Davies ^{2}H ENDOR spectra of RNR intermediate **X** (WT; 33 ms**)** in D_2O (^{2}H). Simulated parameters for the terminal (**see Fig 4A/Table 1**) and bridging hydroxides: ***g*** **=** [$g_1 = 2.0056$, $g_2 = 1.9977$, $g_3 = 1.993$], ***T*** **=** [$T_1 = -3.387$, $T_2 = -0.24$, $T_3 = 3.627$] MHz (Euler angles $\alpha = 3.0^{\circ}$, $\beta = 129.4^{\circ}$, $\gamma = 82.0^{\circ}$).

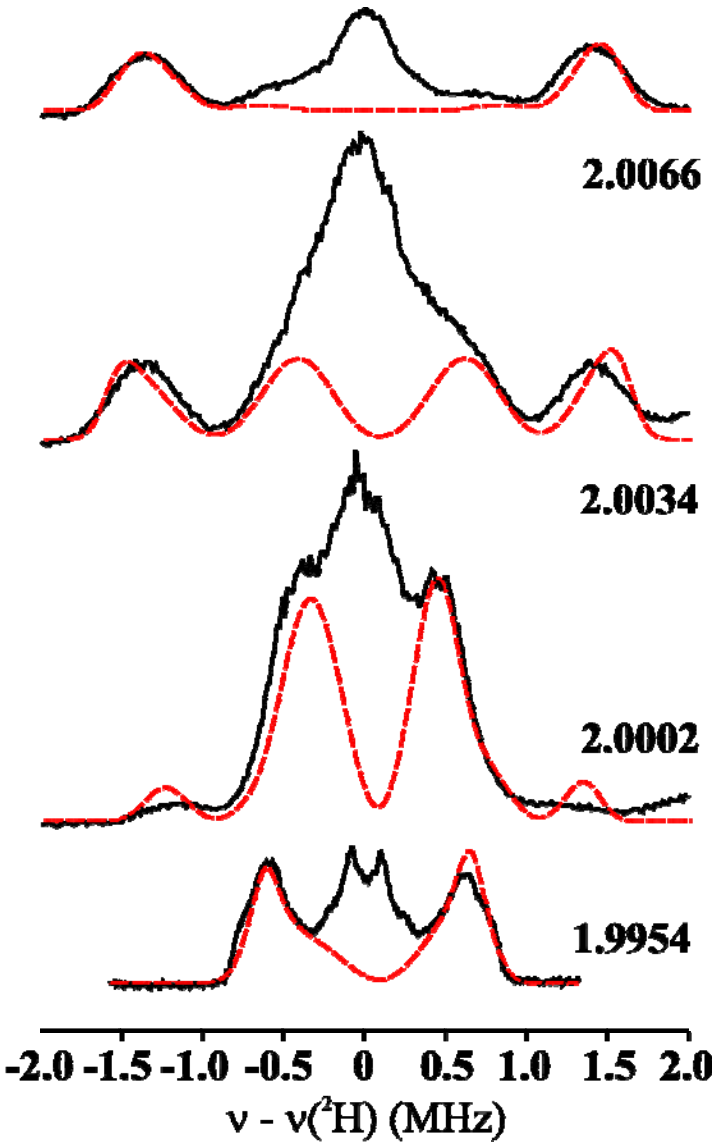

Fig S6:

Simulated (red) and experimental (black) 2-D field-frequency plot of Mims ^{2}H ENDOR spectra of **X**(WT; 33 ms) in D_2O (^{2}H): Conditions: π pulse length = 50 ns, τ = 500 ns, repetition time = 50 ms, MW frequency = 34.949 GHz, T = 2 K. Simulation (with Mims hole; τ = 500 ns) parameters (determined as described in text): $\boldsymbol{g}$ = [g_1 = 2.0056, g_2 = 1.9977, g_3 = 1.993], $\boldsymbol{A}$ = [A_1 = -1.55, A_2 = -1.15, A_3 = 3.2] MHz (Euler angles α = 10.5°, β = 72°, γ = 0), line widths used = 0.1 (minimum) to 0.22 (maximum) MHz. All spectra are centered at the ^{2}H nuclear Larmor frequency.

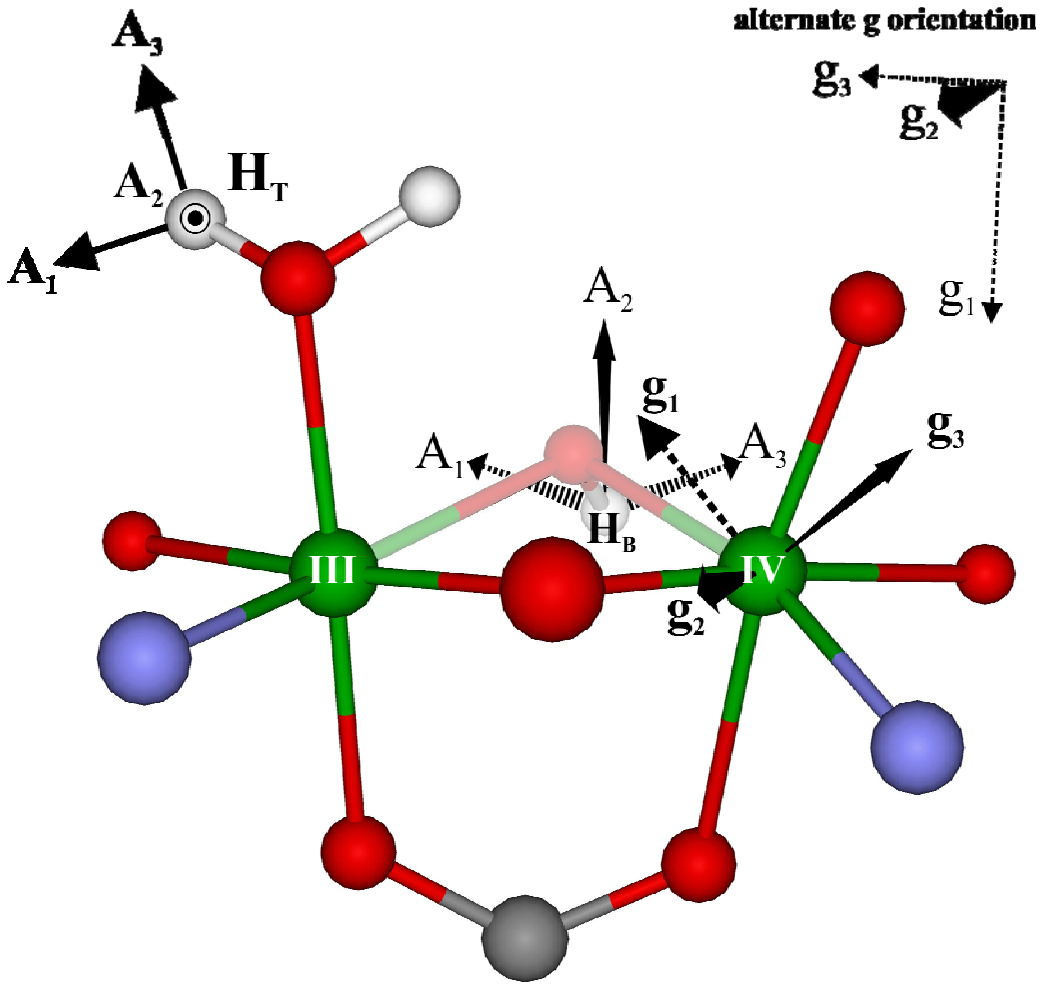

Fig S7:

Orientation of $\boldsymbol{A_T}$, $\boldsymbol{T/A_B}$ for the hypothetical **T(H_T)+B(H_B)** model of **X** (Model 2) considered by HLLN, along with two alternate orientations of $\boldsymbol{g}$ in molecular frame determined from $\boldsymbol{A_T}$ and experimental simulation parameters (See **Supp. Mat**). $\boldsymbol{T_T}$ is not shown for the other terminal proton.

Table S1. Metrical and ^{2}H spin Hamiltonian parameters used to calculate[a] the 2-D ENDOR patterns displayed in **Fig 4A**.

	Terminal OH_X^-			Terminal H_2O (Calculated)[e]	
	Experimental		Optimized[c]	Proton-1	Proton-2
	($\boldsymbol{A^{ex}}$)[b]	($\boldsymbol{T^{ex}}$)	($\boldsymbol{T_T}$)	($\boldsymbol{T}$)	($\boldsymbol{T}$)
A_1/T_1(MHz)	-1.55	-1.717	-1.718	-1.755	-2.047
A_2/T_2(MHz)	-1.15	-1.317	-1.316	-1.563	-1.109
A_3/T_3(MHz)	3.2	3.033	3.034	3.338	3.157
λ		0.132	0.132	0.064	0.297
A_{iso}(MHz)	0.167			0	0
r1(Å)[d]			2.625	2.53	2.64
β (°)			94.5	111.3	75.3
γ (°)			90.0	108.3	68.6
d_{FeFe}(Å)			2.84	2.84	2.84

[a] Simulations employed $g = [g_1, g_2, g_3] = [2.0056, 1.9977, 1.993]$. Quadrupole splitting for ^{2}H (I = 1) are not resolved, their inclusion had no effect on simulations, so were not incorporated.
[b] The Euler angles for $\boldsymbol{A^{ex}}$ are $\alpha = 10.5^o$, $\beta = 72.0^o$ and $\gamma = 0.0^o$.
[c]Best match between $\boldsymbol{T^{ex}}$ and **T** as calculated by **eqs S1-4**.
[d] r_1, β, γ and d_{FeFe} are defined in **Fig 3**.
[e] Metrical parameters to calculate the dipolar tensors of the protons of the terminal H_2O, are taken from the structure of reference HLLN2.

Table S2. Calculated orientation of the dipolar tensors of the HLLN2, **B**-proton, $T_{\mathbf{B}}$ relative to $\boldsymbol{g}$-tensor

frame for each of the two choices of H_2O protons.

Proton-1		Proton-2	
$\beta = +72^{\circ}$	$\beta = -72^{\circ}$	$\beta = +72^{\circ}$	$\beta = -72^{\circ}$
$\alpha = 48.4^{\circ}$ $\beta = 54.8^{\circ}$ $\gamma = 69.5^{\circ}$	$\alpha = 3.0^{\circ}$ $\beta = 129.4^{\circ}$ $\gamma = 82.0^{\circ}$	$\alpha = 175.8^{\circ}$ $\beta = 50.8^{\circ}$ $\gamma = 95.0^{\circ}$	$\alpha = 134.4^{\circ}$ $\beta = 117.8^{\circ}$ $\gamma = 60.8^{\circ}$